

# An Experimental and *ab Initio* CI Study for Charge Transfer Excited States and Their Relaxation in Pyrroloborane Derivatives

C. Cornelissen-Gude and W. Rettig\*

W. Nernst Institut für Physikalische und Theoretische Chemie, Humboldt-Universität Berlin, Bunsenstrasse 1, D-10117 Berlin, Germany

Received: October 30, 1998; In Final Form: February 22, 1999

The fluorescence of dimesityl-pyrroloboranes with different ground state twist angles is investigated by absorption, steady state, and time-resolved fluorescence spectroscopies. Only one strongly Stokes shifted charge transfer fluorescence band is found, characterized by monoexponential decays. This fluorescence is connected with extremely low fluorescence rate constants ( $k_f = (1-2) \times 10^6 \text{ s}^{-1}$ ) which are nearly solvent and temperature independent and indicate the forbidden character of the emission. The pretwisted compound shows reduced  $k_f$  values and only a lengthening of the lifetimes with decreasing temperature whereas the planar compound shows a lifetime maximum (increase followed by decrease) upon cooling. This is interpreted as evidence that the planar compound relaxes to a more twisted structure in the excited state. Large-scale *ab initio* CI calculations on a smaller model system confirm the nearly full charge-transfer character present for all twist angles and the energy minimum in the excited state for twisted geometries.

## Introduction

Dyes exhibiting a large Stokes shift possess applicational advantages in several respects. For example, they can improve the performance of fluorescence solar collectors due to the reduction of unwanted reabsorption processes.<sup>1</sup> Furthermore, they can be used for the development of fluoro-ionophores,<sup>2</sup> i.e., fluorescent probes capable of binding to metal ions selectively and thus can serve to monitor ion concentrations in biological systems or heavy metal ions in wastewater. In these cases, the large Stokes shift offers the advantage that the redshifted probe fluorescence is clearly separable from that of the impurities, which are usually present in biological matrices or wastewater.

In general, large Stokes shifts result from electronic or geometrical relaxation processes of photoexcited molecules. Several different mechanisms are known which produce large Stokes shifts. One of them is the molecular geometry relaxation describable by the TICT (twisted intramolecular charge transfer) model (for reviews see refs 3–5). According to the TICT model, which is of a controversial nature<sup>6</sup> and has originally been introduced for the study of donor–acceptor substituted benzenes, the charge transfer reaction occurring in the excited state is accompanied by a simultaneous twisting motion around the bond connecting the donor and acceptor subunits. Unfortunately, the TICT emission process is usually connected with a reduced value of the transition moment due to the small  $\pi$ -overlap of the strongly twisted arrangement of chromophores.<sup>3,5</sup> This property is counteractive regarding the applicational use, because high fluorescence yields are usually desirable. Meanwhile, however, there are already TICT compounds available possessing large fluorescence quantum yields,<sup>7,8</sup> which allow a new access to the development of fluorescence probes.

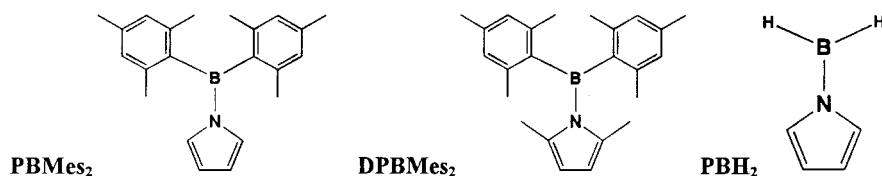
Aminoborane  $\text{H}_2\text{N}-\text{BH}_2$  also represents a donor–acceptor system and has been studied theoretically as model structure for the TICT process using large scale *ab initio* configuration interaction.<sup>9–11</sup> Starting from an excited aminoborane molecule with a planar structure, reached by absorption according to the

Franck–Condon principle, a geometrical relaxation in  $S_1$  takes place leading to an energetic minimum connected with an orthogonal twist of donor with respect to acceptor subunit. The corresponding wave function is strongly dominated by charge transfer contributions. Consequently, the emission originating from this highly polar excited state is expected to exhibit a large Stokes shift and a marked sensitivity to the polarity of the surrounding medium.

Within the scope of this paper, the spectroscopic properties of two borane compounds, closely related to the theoretical TICT model  $\text{H}_2\text{N}-\text{BH}_2$ , are compared to large-scale *ab initio* CI calculations. Experimentally, the B,B-bis(mesityl)pyrroloboranes  $\text{PBMe}_2$  and  $\text{DPBMe}_2$  were chosen, with pyrrole (P) as the donor and a dimesitylborane ( $\text{BMe}_2$ ) acceptor (Scheme 1), because boranes possessing mesityl substituents are commonly known as stable compounds.<sup>12–14</sup> On the theoretical side, the corresponding model system  $\text{PBH}_2$ , where the mesityl groups were replaced by hydrogen atoms (Scheme 1), was investigated.

## Experimental Section

The B,B-bis(mesityl)pyrroloboranes  $\text{PBMe}_2$  and  $\text{DPBMe}_2$  were a gift of D. Britelli and D. F. Eaton. Synthesis and preparation have been described in detail.<sup>15</sup> In their paper, dual fluorescence spectra are reported, which were not identical with the emission spectra observed by our group. We therefore tried to purify the compounds further by repeated recrystallization from *n*-hexane. After this, high-performance thin-layer chromatography (HPTLC)<sup>16,17</sup> still produced evidence for traces of impurities. With a HPTLC plate (type silicagel 60 F254) and a mobile phase of *n*-hexane/diethyl ether (70:1), three different species could be detected. The main component with an absorption maximum for  $\text{PBMe}_2$  at 274 nm ( $\epsilon = 14000 \text{ M}^{-1}\text{cm}^{-1}$  in *n*-hexane) was well separable from the two other ones, which were present in traces only and showed a blue-shifted absorption (260 nm). Using the diagonal separation procedure, i.e., the development of the HPTLC plate into two orthogonal directions, we could exclude that the minor com-

**SCHEME 1: Chemical Structures of the Experimentally (PBMe<sub>2</sub>, DPBMe<sub>2</sub>) and Theoretically (PBH<sub>2</sub>) Studied Pyrroloborane Compounds**


ponents were decomposition products, directly formed during the time of the chromatographic development. Whereas the absorption range of the bis(mesityl)pyrroloboranes coincides with those of the impurities, the energetic range of the fluorescence spectra differs strongly. The impurities produce a short wavelength fluorescence band which, together with the redshifted emission of the boranes, could be taken as dual emission<sup>15</sup> especially since the excitation spectra for the two emission bands are very similar.

A further important point concerns the stability of the bis(mesityl)pyrroloboranes in polar and nonpolar solvents. The thermal and photochemical decomposition of the sample solutions was monitored by absorption. A high degree of thermochemical and photochemical stability of the pyrroloboranes was noted in nonpolar and weakly polar solvents. In strongly polar solution, however, decomposition was observed which results in a strong blue shift of the maximum of the absorption band. Therefore, for the spectroscopic studies every sample solution had to be freshly prepared from the compound purified by thin-layer chromatography.

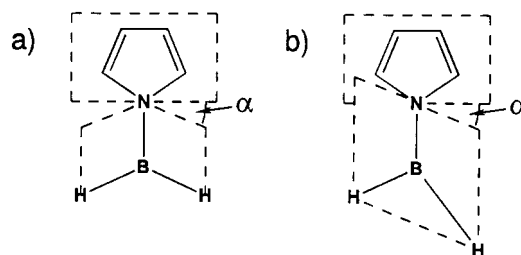
Absorption spectra were measured on a Cary 17 spectrometer and quantum-corrected fluorescence spectra (concentrations  $< 10^{-4}$  M) on a Perkin-Elmer 650–60 fluorimeter.

Basic Blue 3<sup>18</sup> was used as quantum counter to extend the correction range of the emission up to 700 nm. Fluorescence quantum yields were determined relative to a solution of quinine bisulfate in 0.1 N H<sub>2</sub>SO<sub>4</sub> ( $\phi_f = 0.515$ )<sup>19,20</sup> and corrected for the refractive index of the solvents. Fluorescence spectra, measured in aerated solutions, were independent of concentration and excitation wavelength. The determination of low-temperature fluorescence quantum yields took into account the temperature dependence of the refractive index as well as the increasing solvent contraction (density increase) with decreasing temperature.

Fluorescence decay times of the aerated solutions were determined with the time-correlated single-photon counting (SPC) technique<sup>21</sup> using an equipment described elsewhere.<sup>22</sup> Comparative measurements with polarization filters set to the magic angle position were carried out but were not used as standard condition because of the low intensity of the emission. Synchrotron radiation from the Berlin electron storage ring BESSY operating in the single bunch mode was used for excitation.<sup>22,23</sup> The decay times were fitted using the iterative reconvolution procedure (Marquard algorithm), which allowed a time resolution down to 0.1 ns and a relative precision of about 0.1 ns.

Solvents for fluorescence spectroscopy were of Merck Uvasol or Aldrich spectrophotometric grade quality, with the exception of butyronitrile, and were used without further purification. Butyronitrile was purified by column chromatography (Al<sub>2</sub>O<sub>3</sub>) and repeated vacuum distillation.

**Computational Details and Choice of the Reaction Coordinate.** Geometry optimizations have been carried out at the RHF/ROHF level including analytical gradient techniques. Furthermore, a DZ basis set (Huzinaga) was used with the

**SCHEME 2: Schematical Representation of the Symmetry Constraints during Geometry Optimization: (a) C<sub>s</sub>, Symmetry; (b) C<sub>2</sub>, Symmetry**


contraction of Dunning and Hay,<sup>24</sup> (4s, 2s) for H and (9s, 5p; 4s, 2p) for C, B, and N, with one additional polarization function on all atoms (DZP).

For the optimization of selected geometrical parameters of the ground and excited-state geometries, the molecule was fixed in a C<sub>s</sub> or C<sub>2</sub> symmetry. Additionally, the structural parameters of the pyrrolo subunit were taken from the literature and used as fixed values. These geometrical constraints take into account on the one hand the pyramidalization of the borane part (Scheme 2a) and on the other hand the twisting of the BH<sub>2</sub> unit around the BN bond as shown schematically in Scheme 2b.

The resulting most stable geometries for the ground and first excited state are planar and fully twisted (90°) structures, respectively. Further geometry optimization of the S<sub>1</sub> state with a fixed twist angle  $\alpha = 0^\circ$  has been carried out, which corresponds to the excited PBH<sub>2</sub> molecule being fixed in a Franck–Condon type geometry, i.e., after excitation only small geometrical variations (e.g., bond length changes) were allowed. Experimentally, this situation is found in a rigid environment condition.

Single-point CI calculations have been performed using a multireference direct CI<sup>25</sup> and a conventional MR–SDCI<sup>26</sup> method, the latter being particularly suited for the investigation of excited states of systems of low molecular symmetry.

Using a DZP basis set, the molecular basis set consists of 126 atomic orbitals. To restrict the number of generated singly and doubly excited configurations, 12 doubly occupied molecular orbitals were used as a fixed core. Taking into account two or three reference configurations, depending on the state symmetry, more than  $1 \times 10^6$  configuration state functions were generated.

Furthermore, the importance of Rydberg excitations within the absorption spectra of pyrroloborane was checked by CI calculations based on a DZP basis set augmented with a set of very diffuse Rydberg functions localized at the nitrogen atom.<sup>27</sup>

**Results**

**(a) Spectroscopy at Room Temperature.** One of the most remarkable features of the spectroscopy of the B,B-bis(mesityl)pyrroloboranes PBMe<sub>2</sub> and DPBMe<sub>2</sub> is the very large apparent Stokes shift between the absorption maximum and the emission maximum (Figure 1), reaching values of 13100 cm<sup>-1</sup> for

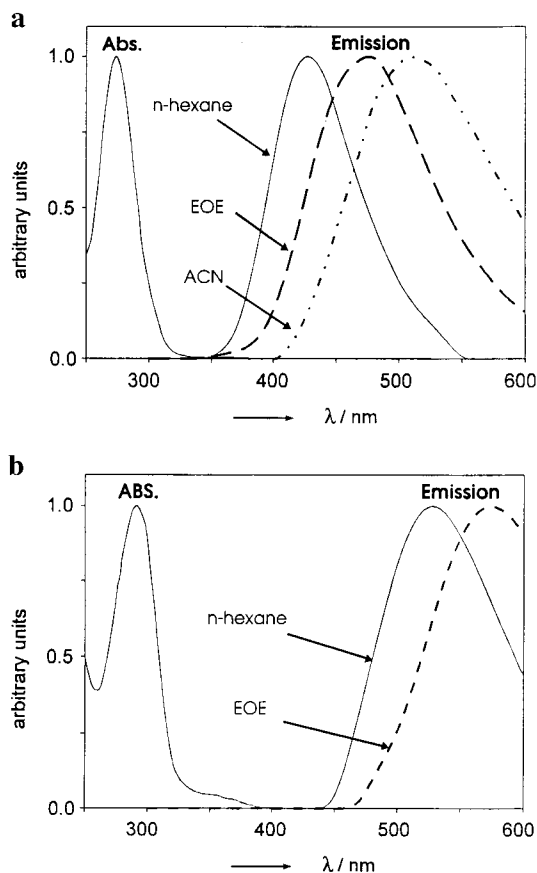


**Figure 1.** Absorption and fluorescence spectra of (a) PBMe<sub>2</sub> and (b) DPBMe<sub>2</sub> at room temperature in solvents of different polarity (EOE = diethyl ether; ACN = acetonitrile).

PBMe<sub>2</sub> and 15800 cm<sup>-1</sup> for DPBMe<sub>2</sub>, even in the nonpolar solvent *n*-hexane. The effect is more strongly pronounced for the dimethyl substituted compound DPBMe<sub>2</sub> (Figure 1). There is also some difference in their absorption spectra. The absorption band of DPBMe<sub>2</sub> is slightly red shifted with respect to that of PBMe<sub>2</sub> and exhibits a weak shoulder on the red edge which was also observed in the excitation spectra.

The absorption maxima of both compounds are insensitive to changes of solvent polarity, but the fluorescence exhibits significant solvatochromic effects indicating that the emission originates from a charge transfer state. In the case of DPBMe<sub>2</sub> the strong red shift of the emission band in solvents of high polarity is accompanied by a loss of fluorescence intensity.

The fluorescence decay curves are monoexponential within the time limitation of our instrument (0.1 ns), which allows the evaluation of radiative and nonradiative rate constants according to eqs 1 and 2, where  $k_{nr}^{tot}$  corresponds to the sum of all nonradiative processes including population of the triplet state.

$$k_f = \phi_f / \tau_f \quad (1)$$

$$k_{nr}^{tot} = k_f(\phi_f^{-1} - 1) \quad (2)$$

The measured data and calculated photophysical rates are collected in Table 1.

Apart from the larger value of the Stokes shift, the compound DPBMe<sub>2</sub> differs from PBMe<sub>2</sub> by the observed fluorescence intensity, which vanishes in highly polar solvents. The radiative rate constants  $k_f$  are extremely small and decrease with increasing solvent polarity (Table 1). The corresponding radiative lifetimes  $\tau_f = k_f^{-1}$  are thus very long and even lengthened

**TABLE 1: Spectral and Photophysical Data at Room Temperature for (a) PBMe<sub>2</sub> and (b) DPBMe<sub>2</sub> in Solvents of Different Polarity**

solvent	$\lambda_{max}^{em}/nm$	$\Delta\nu_{St}/cm^{-1}$	$\phi_f$	$\tau_f/ns$	$k_f/s^{-1}$	$k_{nr}/s^{-1}$
(a) PBMe <sub>2</sub> ( $\lambda_{max}^{abs} = 274 nm$ )						
<i>n</i> -hexane	428	13100	0.015	7.4	$2.0 \times 10^6$	$13.3 \times 10^7$
dibutylether	455	14500	0.024	15	$1.6 \times 10^6$	$6.5 \times 10^7$
diethylether	475	15400	0.038	30	$1.30 \times 10^6$	$3.2 \times 10^7$
butyronitrile	497	16400	0.020	18	$1.10 \times 10^6$	$5.4 \times 10^7$
ethanol	495	16300	0.020	19	$1.05 \times 10^6$	$5.2 \times 10^7$
acetonitrile	510	16900	0.018	16	$1.15 \times 10^6$	$6.1 \times 10^7$
(b) DPBMe <sub>2</sub> ( $\lambda_{max}^{abs} = 291 nm$ )						
<i>n</i> -hexane	538	15800	0.012	13.6	$8.8 \times 10^5$	$7.3 \times 10^7$
dibutylether	566	16700	0.006	8.5	$7.0 \times 10^5$	$11.7 \times 10^7$
diethylether	580	17100	0.004	5.5	$8.0 \times 10^5$	$18.1 \times 10^7$
dichloromethane	610	1800	0.002			
butyronitrile				no fluorescence		
acetonitrile				observable at room temperature		

for DPBMe<sub>2</sub> by a factor of 2 as compared to PBMe<sub>2</sub>, reaching values larger than 1000 ns. This enlargement is possibly due to the sterical hindrance by the *ortho* methyl groups, which force the molecular geometry into a more twisted conformation. The long radiative lifetimes of PBMe<sub>2</sub> and DPBMe<sub>2</sub> can be compared to the emission of TICT compounds which is generally known to exhibit a highly forbidden character.<sup>3,5</sup> Within the TICT model, the stronger red shift of the fluorescence spectra of DPBMe<sub>2</sub> is understandable by the better donor ability of the *ortho*-methyl substituted pyrrol ring, a fact supported by photoelectron-spectroscopic data.<sup>28,29</sup> From the difference of their donor ionization energies (0.7–0.8 eV), a red shift of  $\approx 6000 cm^{-1}$  would be expected if the emission is of pure CT character. Experimentally, a red shift of  $\approx 5000 cm^{-1}$  is observed in alkanes, supporting the CT assignment.

By means of the Lippert–Mataga equation (eq 3a),<sup>30–32</sup> an estimation of the excited state dipole moment can be given. Rigorously speaking, this equation cannot be applied for cases where absorption and emission processes correspond to different excited states, which is the case for nearly all TICT compounds. The alternative treatment of the fluorescence alone (Mataga equation, eq 3b), however, leads to identical excited-state dipole moments if the absorption spectra are solvent insensitive, as observed here, and the ground-state dipole moment can be neglected.<sup>33</sup>

$$\Delta\tilde{\nu} = \tilde{\nu}_{abs} - \tilde{\nu}_f = \frac{2\Delta f}{hca^3}(\mu_{s_1} - \mu_{s_0})^2 + const \quad (3a)$$

with

$$\Delta f = \frac{(\epsilon - 1)}{(2\epsilon + 1)} - \frac{(n^2 - 1)}{(2n^2 + 1)}$$

$$\tilde{\nu}_f = -\frac{2\Delta f}{hca^3}\mu_{s_1}(\mu_{s_1} - \mu_{s_0}) + const' \quad (3b)$$

with

$$\Delta f = \frac{(\epsilon - 1)}{(2\epsilon + 1)} - \frac{1}{2} \frac{(n^2 - 1)}{(2n^2 + 1)}$$

The Onsager radii were evaluated by the mass–density formula 4.<sup>34,35</sup>

$$a = \sqrt[3]{3M/4\pi N_A \rho} \quad (4)$$

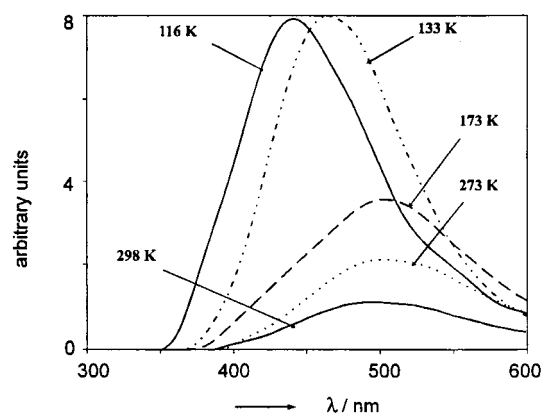


**Figure 2.** Low-temperature effects on the fluorescence spectra of PBMe<sub>2</sub> in ethanol.

**TABLE 2: Temperature Dependence of Photophysical Data of (a) PBMe<sub>2</sub> and (b) DPBMe<sub>2</sub> in the Solvent Mixture Methylcyclohexane:Isopentane (1:4) and Ethanol**

(a) PBMe <sub>2</sub> ( $\lambda_{\text{max}}^{\text{abs}} = 274 \text{ nm}$ )									
T/K	MCH/IPE				EtOH				
	$\lambda_{\text{max}}^{\text{em}}/\text{nm}$	$\phi_f$	$\tau_f/\text{ns}$	$k_{\text{nr}}^a \times 10^8 \text{ s}^{-1}$	$\lambda_{\text{max}}^{\text{em}}/\text{nm}$	$\phi_f$	$\tau_f/\text{ns}$	$k_{\text{nr}}^b \times 10^8 \text{ s}^{-1}$	
298	428	0.015	7.9	1.24	495	0.020	18.5	0.53	
273	430	0.020	9.3	1.05	499	0.025	22.7	0.43	
253	432	0.019	11.1	0.88	502	0.029	25.6	0.37	
233	434	0.024			502	0.041			
213	435	0.022	14.2	0.69	505	0.046	35.6	0.27	
193	435	0.026			504	0.050			
173	436	0.030	14.9	0.65	499	0.064	46.1	0.20	
133	438	0.040	18.5	0.52	458	0.076	55.8	0.17	
116	429	0.042			429	0.084			
77	415				450		16.8		

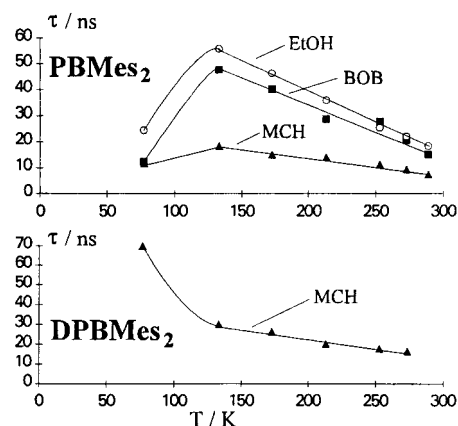
  

(b) DPBMe <sub>2</sub> ( $\lambda_{\text{max}}^{\text{abs}} = 291 \text{ nm}$ )									
T/K	MCH/IPE				EtOH				
	$\lambda_{\text{max}}^{\text{em}}/\text{nm}$	$\phi_f$	$\tau_f/\text{ns}$	$k_{\text{nr}}^c \times 10^8 \text{ s}^{-1}$	$\lambda_{\text{max}}^{\text{em}}/\text{nm}$	$\phi_f$	$\tau_f/\text{ns}$		
298	539	0.011							
273	539	0.012	16.4	0.60					
253	538	0.012	17.8	0.56					
233	540	0.015							
213	542	0.015	20.6	0.48					
193	544	0.016							
173	551	0.018	26.8	0.37					
133	555	0.021	30.3	0.32	571	0.003			
116	546	0.044			522	0.034			
77	500		70.0		512				

<sup>a</sup> The  $k_f$  values were nearly temperature independent, with an average value  $k_f = 2.0 \times 10^6 \text{ s}^{-1}$  for PBMe<sub>2</sub> in MCH/IPE. <sup>b</sup>  $k_f = 1.2 \times 10^6 \text{ s}^{-1}$  for PBMe<sub>2</sub> in EtOH. <sup>c</sup>  $k_f = 7.0 \times 10^5 \text{ s}^{-1}$  for DPBMe<sub>2</sub> in MCH/IPE.

We used  $a = 5.08 \text{ \AA}$  and  $a = 5.23 \text{ \AA}$ , for PBMe<sub>2</sub> and DPBMe<sub>2</sub>, respectively. With the observed solvatochromic slopes based on the data in Table 1,  $m(\text{PBMe}_2) = 11.4 \times 10^3 \text{ cm}^{-1}$  and  $m(\text{DPBMe}_2) = 9.4 \times 10^3 \text{ cm}^{-1}$ , the dipole moments were calculated to be 17.2 D for PBMe<sub>2</sub> and 16.3 D for DPBMe<sub>2</sub>, i.e., very large but of comparable magnitude.

**(b) Spectroscopic Measurements at Low Temperature.** Emission spectra have been measured in the temperature range from 298 K to 77 K. The temperature effects have been studied in the nonpolar solvent mixture methylcyclohexane:isopentane (MCH:IPE) as well as in polar ethanol. Upon lowering the temperature, a weak redshift of the fluorescence maxima can be observed (Table 2), explainable by the increasing dielectric



**Figure 3.** Temperature dependence of the fluorescence lifetimes of PBMe<sub>2</sub> and DPBMe<sub>2</sub> in solvents of different polarity (MCH = methylcyclohexane/isopentane (1:4), BOB = di-*n*-butyl ether, EtOH = ethanol).

**TABLE 3: Arrhenius Parameters (Activation Energy  $E_a$ , Preexponential Factor  $k_{\text{nr}}^{\infty}$  and Correlation Coefficient  $\langle r \rangle$ ) for PBMe<sub>2</sub> and DPBMe<sub>2</sub> in the Solvent Mixture Methylcyclohexane/Isopropane (1:4) and in Ethanol**

		$E_a/\text{kJ mol}^{-1}$	$k_{\text{nr}}^{\infty}/\text{s}^{-1}$	$\langle r \rangle$
PBMe <sub>2</sub>	in MCH/IPE	3.64	$5.2 \times 10^8$	0.978
	in EtOH	3.23	$1.8 \times 10^8$	0.970
DPBMe <sub>2</sub>	in MCH/IPE	1.92	$1.4 \times 10^8$	0.998

constant  $\epsilon(T)$  of the solvent. For temperatures below the melting point of the solvent, a hypsochromic shift of the emission band occurs. This temperature behavior is exemplified for PBMe<sub>2</sub> in ethanol (Figure 2). The blue shift below 173 K results from the freezing out of solvent relaxation processes,<sup>36</sup> preventing the stabilization of the solute charge transfer state. This effect is also observed for MCH:IPE as solvent, although at lower temperature (Table 2).

The photophysical data of PBMe<sub>2</sub> and DPBMe<sub>2</sub> measured at different temperatures are collected in Table 2a,b. For DPBMe<sub>2</sub> in ethanol, fluorescence is observable only for temperatures below 133 K, and increases strongly with decreasing temperature. Consequently, the process connected with the nonradiative deactivation of the excited state can be frozen out at very low temperatures.

On the basis of the temperature-dependent values of the fluorescence quantum yields and lifetimes, an evaluation of the rate constants  $k_{\text{nr}}$  and  $k_f$  was carried out, using eqs 1 and 2.

The nonradiative rate constant  $k_{\text{nr}}(T)$  shows a strong decrease with lowering temperature, whereas the  $k_f$  values remain almost temperature independent. From a plot of  $k_{\text{nr}}(T)$  versus  $1/T$  according to the Arrhenius eq 5, the activation energies and preexponential factors can be determined and are collected in Table 3.

$$k_{\text{nr}}^{\text{tot}}(T) = k_{\text{nr}}^{\infty} \exp(\Delta E_A/RT) \quad (5)$$

A significantly lower activation energy is found for the dimethyl pyrrolo compound DPBMe<sub>2</sub> as compared to PBMe<sub>2</sub>, and there is no obvious solvent polarity dependence observable.

The fluorescence decay times, which were exclusively monoexponential, exhibit a qualitatively different temperature dependence for both pyrroloboranes (Figure 3). The fluorescence lifetimes of PBMe<sub>2</sub> possess a maximum value around 140 K, with the  $\tau$  value at 77 K being considerably smaller. This has to be interpreted by a change of  $k_f$ , i.e., a change of the character of the emitting state, if an increase of  $k_{\text{nr}}$  for low temperatures

**TABLE 4: Direct CI/(DZP) Energies for the Singlet  $S_0$ ,  $S_1$ ,  $S_2$  and the Triplet  $T_1, T_2$  States of PBH<sub>2</sub> in the Optimized Planar Ground State Geometry**

state	energy/au	$\Delta E_{\text{abs}}/\text{eV}$	$\Delta E_{\text{abs}}/\text{nm}$	$\mu/\text{D}$	$f$
$S_0$	1 <sup>1</sup> A	-234.484 480			0.28
$S_1$	1 <sup>1</sup> B	-234.313 702	4.65 <sup>a</sup>	267 <sup>a</sup>	7.75 0.08
$S_2$	2 <sup>1</sup> A	-234.265 271	5.97 <sup>a</sup>	209 <sup>a</sup>	4.25 0.12
$T_1$	1 <sup>3</sup> B	-234.355 131	3.52 <sup>a</sup>	352 <sup>a</sup>	2.51
$T_2$	1 <sup>3</sup> A	-234.302 146	4.96 <sup>a</sup>	250 <sup>a</sup>	5.75

<sup>a</sup> Referring to the ground state energy  $E(S_0)$  of the  $S_0$  optimized geometry.

is ruled out. Such lifetime maxima have previously been found for donor–acceptor stilbenes<sup>8</sup> and were interpreted as evidence for state switching. Unfortunately, a direct proof of the increased  $k_f$  values at 77 K could not be done because the  $\phi_f$  values at 77 K could not be determined.

Contrary to the behavior of PBMe<sub>2</sub>, the lifetime values of the dimethyl-substituted pyrrolo compound DPBMe<sub>2</sub> increase monotonically upon cooling, caused by reduction of a temperature dependent nonradiative process, and possess a highest value at 77 K indicating a very strongly forbidden emission (compare the low  $k_f$  values in Tables 1 and 2). At temperatures above 130 K, the decay times of both compounds in MCH:IPE become similar. This can be understood by the above-mentioned state switching for PBMe<sub>2</sub>, which is consistent with a geometrical relaxation process for this compound, which can be frozen out and which leads to a larger twist-angle as inherent for DPBMe<sub>2</sub>. Therefore, at 77 K, the emission of PBMe<sub>2</sub> should originate from the geometrically unrelaxed Franck–Condon state connected with a shorter radiative lifetime. Due to the sterical hindrance of the ortho methyl groups, the conformation of DPBMe<sub>2</sub> is more strongly twisted in the ground state and frozen excited state. The results at 77 K indicate, that  $k_f$  should be angle dependent, with a reduction for larger twist angles.

**(c) Ab Initio Calculations.** Apart from the spectroscopic investigations of the B,B-bis(mesityl)pyrrolboranes PBMe<sub>2</sub> and DPBMe<sub>2</sub>, an ab initio large-scale CI study of a corresponding model PBH<sub>2</sub> (Scheme 1) has been performed. Different types of symmetry constraints ( $C_{2v}$ ,  $C_2$ ,  $C_s$ ) which allow several distinct relaxation processes were taken into account, especially regarding twisting movements ( $C_2$ ) and pyramidalisation effects ( $C_s$ ) (Scheme 2). The geometry optimization of the model system shows, however, that regardless of the symmetry constraint, a planar structure of the ground-state molecule is favored. Using this geometry as starting point, the absorption spectra were calculated, assuming vertical transitions. The variation of basis sets shows clearly that Rydberg states do not contribute to the low lying transitions of PBH<sub>2</sub>. The CI energy values, the calculated dipole moments, and the oscillator strengths of the ground and the excited states for the planar  $S_0$  conformation are collected in Table 4.

The  $S_1$  state possesses a dipole moment of around 8 D and can be characterized by an electron-transfer process from the pyrrolo unit to the boron atom. Although this dipole moment is much smaller than the experimental one ( $\approx 17$  D) due to the neglect of the mesityl groups in the calculation, its considerable size means that  $S_1$  corresponds to a pure charge transfer state even for the planar geometry. This behavior is contrary to that of the TICT model aminoborane H<sub>2</sub>N–BH<sub>2</sub><sup>9,10</sup> and to the experimental results for the prototype of TICT molecules, dimethylaminobenzonitrile (DMABN).<sup>3–5,33</sup>

The oscillator strength calculated for the  $S_0 \rightarrow S_1$  transition for the planar structure is rather small ( $f = 0.08$ ). The energy

**TABLE 5: Direct CI/(DZP) Energies for the Singlet  $S_0$ ,  $S_1$  and the Triplet  $T_1$  State of PBH<sub>2</sub> for the Planar and the 90° Twisted Conformation Optimized in the  $S_1$  Excited State**

geometry	state	energy/au	$\Delta E/\text{eV}$	$\Delta E/\text{nm}$	$\mu/\text{D}$
planar ( $\alpha \approx 0^\circ$ )	$S_0$	1 <sup>1</sup> A	-234.466 582	0.49 <sup>a</sup>	1.48
	$S_1$	1 <sup>1</sup> B	-234.323 126	3.91 <sup>b</sup>	318 <sup>b</sup> 7.44
	$T_1$	1 <sup>3</sup> B	234.341 688	3.40 <sup>b</sup>	365 <sup>b</sup> 5.17
twisted $\alpha \approx 90^\circ$	$S_0$	1 <sup>1</sup> A	-234.436 042	1.32 <sup>a</sup>	2.48
	$S_1$	1 <sup>1</sup> B	-234.329 591	2.89 <sup>c</sup>	430 <sup>c</sup> 7.31
	$T_1$	1 <sup>3</sup> B	-234.330 941	2.86 <sup>c</sup>	433 <sup>c</sup> 7.28

<sup>a</sup> Energy difference of the Franck–Condon ground state referring to  $E(S_0)$  in a geometry optimized for the planar ground state ( $\alpha \approx 0^\circ$ ).  
<sup>b</sup> Referring to  $E(S_0)$  in a geometry optimized for the planar  $S_1$  state ( $\alpha \approx 0^\circ$ ).  
<sup>c</sup> Referring to  $E(S_0)$  in a geometry optimized for the twisted  $S_1$  state ( $\alpha \approx 90^\circ$ ).

differences connected with the  $S_0 \rightarrow S_1$  and  $S_0 \rightarrow S_2$  transitions were calculated as 4.65 eV (267 nm) and 5.97 eV (209 nm). The comparison of the  $S_0 \rightarrow S_1$  transition energy of the model compound PBH<sub>2</sub> and the observed band maximum of PBMe<sub>2</sub> (274 nm) shows a quite satisfactory agreement. But the energy range of the second transition, i.e., that calculated for the  $S_2$  state of PBH<sub>2</sub>, is considered to correspond to a high-lying excited state of the experimental system PBMe<sub>2</sub>, which possesses lower lying locally excited (<sup>1</sup>L<sub>a</sub> and <sup>1</sup>L<sub>b</sub> type) states of the mesityl substituents which should be situated around 260 and 290 nm<sup>37</sup> and which are not included in the calculation. We therefore expect the LE and CT state to be situated in the same energy range for the experimental system PBMe<sub>2</sub>. For DPBMe<sub>2</sub>, where the CT state will be red shifted by 0.54 eV by comparison of the ionization potentials of the corresponding pyrrolo moieties,<sup>28,38</sup> the long wavelength shoulder at 350 nm in the absorption spectrum of DPBMe<sub>2</sub> (Figure 1b) is therefore interpreted to correspond to the CT state, because the local excitations of the mesityl groups (absorption maximum at 291 nm) are not expected to shift into this energy range.

To simulate the geometrical relaxation process, which takes place during the lifetime of the excited molecule, a geometry optimization of the first excited state has been carried out. The symmetry was restricted to the point group  $C_2$ , allowing molecular rotations around the BN bond, but not pyramidalization movements at the B and N centers. Analogous to the H<sub>2</sub>N–BH<sub>2</sub> system, the  $S_1$  minimum was found at the orthogonally twisted geometry for PBH<sub>2</sub>. Consequently, the first singlet excited state can also be characterized as a TICT state with a perpendicular minimum. This is further confirmed by the energetic proximity of the corresponding triplet state (Table 5). Furthermore, a geometry optimization of the  $S_1$  state restricted to the planar conformation ( $\alpha = 0^\circ$ ) was carried out. Within these geometrical constraints (fixed angles  $\alpha = 0^\circ$  or  $\alpha = 90^\circ$ ), the optimized excited-state structures differ from the ground-state geometry by a significant lengthening of the BN bond from 1.44 to 1.61 Å. A comparison of energies and dipole moments for the optimized planar and perpendicular molecule in the excited state is given in Table 5, and the optimized structures are summarized in Table 6.

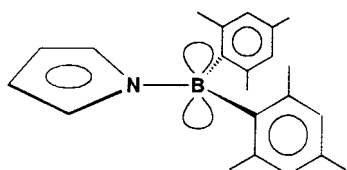
In contrast to the  $S_0 \rightarrow S_1$  transition energy (4.65 eV referred to the planar ground state geometry), corresponding to the CT absorption process in sterically unhindered compounds, the  $S_0/S_1$  energy gap of the optimized twisted structure possesses a remarkably lower value (2.89 eV). The corresponding redshift of the fluorescence energy is to a large extent caused by the strong destabilization of the twisted ground-state molecule (1.32 eV).

The dipole moments of the  $S_1$  state in the planar and twisted conformation are almost identical due to the twist angle

**TABLE 6: Selected Geometrical Parameters Resulting from the Geometry Optimization of the  $S_0$  Ground and First Excited State  $S_1$** 

parameter	$S_0^a$	$S_1^a$	$S_1^b$
$r(\text{BN})/\text{\AA}$	1.441	1.608	1.613
$r(\text{BH})/\text{\AA}$	1.185	1.191	1.189
$\omega(\text{NBH})$	$118.9^\circ$	$114.9^\circ$	$113.8^\circ$
$\alpha(\text{CNBH})^c$	$0^\circ$	$90^\circ$	$0^\circ$

<sup>a</sup> Full optimization of all geometrical parameters around the boron atom. <sup>b</sup> Fixed twist angle during geometry optimization. <sup>c</sup> Twist angle, see Scheme 2b; pyramidalization was found negligible in all cases.

**SCHEME 3: Model of the Geometrical Arrangement of  $\pi$ -Systems in PBMe<sub>2</sub>**

independent decoupling<sup>29,39</sup> of the boron and the pyrrolo unit, contributing to the charge transfer as outlined above.

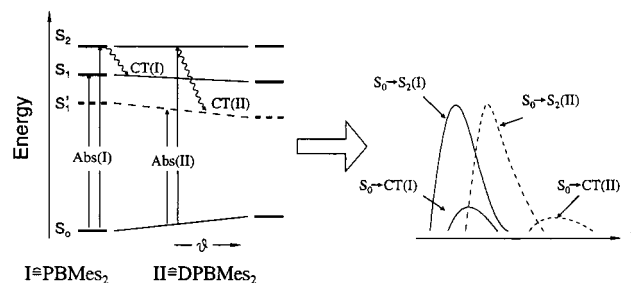
### Discussion

Although the experimental and the calculated *ab initio* transition energies agree satisfactorily, the question should be considered if the theoretical model compound PBH<sub>2</sub> allows an adequate description of the pyrroloborane PBMe<sub>2</sub>, studied experimentally. There are two points of particular importance. One of them concerns the planarity of the pyrroloborane system in the ground state. Moreover, the effect of the exchange of the mesityl groups by hydrogen atoms in the calculated model compound should be discussed.

There are numerous experimental investigations available in the literature referring to these points. Dynamical <sup>1</sup>H NMR<sup>40–42</sup> and <sup>13</sup>C NMR<sup>43–46</sup> measurements, investigations by means of electrochemical cyclic voltammetry,<sup>47</sup> <sup>11</sup>B and <sup>14</sup>N NMR<sup>48,49</sup> as well as X-ray studies<sup>50–52</sup> have been performed for several triarylboranes, pyrroloboranes, and aminoborane derivatives. Most of them indicate the existence of a structure analogous to that given in Scheme 3, i.e., corresponding to an almost planar pyrroloborane unit with twisted mesityl substituents.<sup>43–52</sup> The twist angle varies strongly and is generally assumed to be situated in the range  $50^\circ$ – $90^\circ$ . This twisted geometry should prevent a strong coupling between the locally excited states of the mesityl groups and the charge transfer state, the energy level of which is considered to be very close lying.

Summarizing all theoretical and experimental aspects regarding the spectroscopic features of the pyrroloboranes, the following interpretation can be proposed: In view of (i) the occurrence of a large fluorescence red shift in nonpolar and even in rigid media (Figure 2), (ii) the low value of the oscillator strength as calculated for the  $S_0 \rightarrow \text{CT}$  transition and the low fluorescence intensity found experimentally, (iii) the energetic neighborhood of the CT state and the locally excited state of the mesityl group (LE), it can be assumed that the experimentally observed absorption band of PBMe<sub>2</sub> has to be characterized as a superposition of a forbidden  $S_0 \rightarrow S_1$  (CT) and a more allowed  $S_0 \rightarrow S_2$  (LE) transition. These assumptions are schematically depicted in Scheme 4.

For PBMe<sub>2</sub>, possessing a planar conformation in the ground state, the CT transition is hidden by the stronger  $S_0 \rightarrow S_2$  (LE) absorption band. The maxima of these absorption transitions, however, are expected to be better separated for DPBMe<sub>2</sub>.

**SCHEME 4: Schematic Model Explaining the Absorption Bands of PBMe<sub>2</sub> and DPBMe<sub>2</sub>: (—) Singlet States of PBMe<sub>2</sub> and (---) Singlet States of DPBMe<sub>2</sub>**

Because of the methyl groups on the pyrrolo moiety in DPBMe<sub>2</sub>, the donor capability is increased by 0.55 eV<sup>28</sup> leading to a stronger stabilization of the CT state. Furthermore, the dimethyl substituted compound DPBMe<sub>2</sub> should be more strongly twisted in the ground state in comparison to PBMe<sub>2</sub>, reflected in a reduced  $S_0 \rightarrow \text{CT}$  transition moment, i.e., decreased CT absorption intensity. Both points justify the assignment of the weak shoulder in the red edge of the absorption spectrum of DPBMe<sub>2</sub> to the  $S_0 \rightarrow \text{CT}$  transition. The emission originates exclusively from a highly polar excited state as is evidenced by the strong solvatochromic effects (Figure 1a,b).

Therefore, the strongly anomalous Stokes shift of the B,B-bis(mesityl)pyrroloboranes PBMe<sub>2</sub> and DPBMe<sub>2</sub>, as measured with respect to the absorption maximum, can be interpreted as resulting partly from the energy loss due to the internal  $S_2 \rightarrow S_1$  conversion processes, partly from the intramolecular geometrical and partly from the dipolar solvent relaxation.

There are both experimental and theoretical indications for the existence of an intramolecular geometrical relaxation process. Moreover, the comparison of the low-temperature fluorescence lifetimes for PBMe<sub>2</sub> and DPBMe<sub>2</sub> as well as the calculated relative energies of the optimized  $S_1$  state of the model compound PBH<sub>2</sub> indicate a connection of this geometrical relaxation with the twisting motion around the B–N bond.

This twisting relaxation is a large amplitude motion in PBMe<sub>2</sub> which can be stopped in low-temperature frozen solvent matrix at 77 K and which produces the lifetime maximum observed for PBMe<sub>2</sub> in Figure 3 for temperatures where the matrix is soft enough to allow for the geometrical relaxation. The lengthened lifetime upon temperature increase from 77 to 130 K is an indication that the geometry relaxation leads toward a conformation of reduced transition moment, such as the twisting process. A nonradiative process always shortens the fluorescence decays and cannot be the cause of such a lifetime lengthening. A similar lifetime maximum has been observed in the case of a donor–acceptor stilbene.<sup>8</sup> An additional relaxation component could be connected with a small-amplitude motion because part of the anomalously large Stokes shift remains in frozen solvents (Figure 2) and even at 77 K (Table 2). Such a small amplitude motion could be the variation of the B–N bond length as indicated by the calculations.

**Acknowledgment.** We wish to thank D.R. Britelli and D.F. Eaton for the gift of the compounds. This work has been supported by the Bundesministerium f. Forschung und Technologie Project 05 414 SKT as well as by the Deutsche Forschungsgemeinschaft within SFB337. The computational support and fruitful discussions with V. Bonačić-Koutecký are gratefully acknowledged.

## References and Notes

- (1) Vollmer, F.; Rettig, W. *J. Photochem. Photobiol. A* **1996**, *95*, 143.
- (2) Rettig, W.; Lapouyade, R. In *Topics in Fluorescence Spectroscopy, Vol 4: Probe Design and Chemical Sensing*; Lakowicz, J. R., Ed.; Plenum Press: New York, 1994; p 109.
- (3) Grabowski, Z. R.; Rotkiewicz, K.; Siemiarz, A.; Cowley, D. J.; Baumann, W. *Nouv. J. Chim.* **1979**, *3*, 443.
- (4) Lippert, E.; Rettig, W.; Bonačić-Koutecký, V.; Heisel F.; Miehé, J. A. *Adv. Chem. Phys.* **1987**, *68*, 1.
- (5) Rettig, W. *Angew. Chem., Int. Ed. Engl.* **1986**, *25*, 971. Rettig, W. In *Topics in Current Chemistry, Vol. 169: Electron-Transfer I*; Mattay, J., Ed.; Springer-Verlag: Berlin, 1994; p 253.
- (6) Zachariasse, K. A.; von der Haar, T.; Hebecker, A.; Leinhos, U.; Kühnle, W.; *Pure Appl. Chem.* **1993**, *65*, 1745. von der Haar, T.; Hebecker, A.; Il'ichev, Y.; Jiang, Y. B.; Kühnle, W.; Zachariasse, K. A. *Recl. Trav. Chim. Pays-Bas* **1995**, *114*, 430.
- (7) Dobkowski, J.; Grabowski, Z. R.; Paepow, B.; Rettig, W.; Koch, K. H.; Müllen, K.; Lapouyade, R. *New J. Chem.* **1994**, *18*, 525.
- (8) Lapouyade, R.; Czeschka, K.; Majenz, W.; Rettig, W.; Gilabert, E.; Rullière, C. *J. Phys. Chem.* **1992**, *96*, 9643.
- (9) Bonačić-Koutecký, V.; Michl, J. *J. Am. Chem. Soc.* **1985**, *107*, 1765.
- (10) Michl, J.; Bonačić-Koutecký, V. in *Electronic Aspects of Organic Photochemistry*; Michl, J.; Bonačić-Koutecký, V., Eds.; J. Wiley & Sons: New York, 1990.
- (11) Bonačić-Koutecký, V.; Schöffel, K.; Michl, J. *J. Am. Chem. Soc.* **1989**, *111*, 6140.
- (12) Brown, H. C.; Dodson, V. H. *J. Am. Chem. Soc.* **1957**, *79*, 2303.
- (13) Doty, J. C.; Grisdale, P. J.; Evans, T. R.; Williams, J. L. R. *J. Organomet. Chem.* **1971**, *2*, C35.
- (14) Williams, J. L. R.; Grisdale P. G.; Doty, J. C. *J. Am. Chem. Soc.* **1967**, *89*, 4538.
- (15) Britelli D. R.; Eaton, D. F. *J. Phys. Org. Chem.* **1989**, *2*, 89.
- (16) Frey, H.-P.; Zieloff, K. in *Qualitative and quantitative Dünnschicht-chromato-graphie*; Verlag Chemie: Berlin: 1993.
- (17) Bauer, K.; Gros, Leo; Sauer, W. In *Dünnschicht Chromatographie, -Einführung*; Merck, Fa., Hüthig, A., Eds.; Verlag: Berlin, 1989.
- (18) Heinze, J.; Kopf, U. *Anal. Chem.* **1984**, *56*, 1931.
- (19) Meech, S. R.; Phillips, D. *J. Photochem.* **1983**, *23*, 193.
- (20) Velapoldi, R. A.; Epstein, M. S. *ACS Symp. Ser.* **1989**, *383*, 98.
- (21) O'Connor, D. V.; Phillips, D. In *Time Correlated Single Photon Counting*; O'Connor, D. V., Phillips, D., Eds.; Academic Press: London, 1984.
- (22) Vogel, M.; Rettig, W. *Ber. Bunsen-Ges. Phys. Chem.* **1987**, *91*, 1241.
- (23) Rettig, W.; Wiggerhauser, H.; Hebert, T.; Ding, A. *Nucl. Instrum. Methods Phys. Res.* **1989**, *A277*, 677.
- (24) Dunning, T. H.; Hay, P. J. In *Methods of Electronic Structure Theory*; Schaefer, H. F., Ed.; Plenum Press: New York, 1977; p 1.
- (25) Roos, B. O.; Siegbahn, P. E. M. in *Methods of Electronic Structure Theory*; Schaefer, H. F., Ed.; Plenum Press: New York, 1977; Chapter 7, p 277.
- (26) Buenker, R. J. In *Studies in Physics and Theoretical Chemistry (Current Aspects of Quantum Chemistry 1981)*; Elsevier: Amsterdam, 1982; p 17.
- (27) Bruna, P. J.; Peyerimhoff, S. *Ab Initio Methods in Quantum Chemistry, Vol. I, Excited-State Potentials*; Lawley, K. P., Ed.; John Wiley & Sons Ltd.: New York, 1987.
- (28) Rettig, W.; Marschner, F. *Nouv. J. Chim.* **1983**, *7*, 425.
- (29) Rettig, W.; Marschner, F. *New J. Chem.* **1990**, *14*, 819.
- (30) Lippert, E. *Z. Naturforsch.* **1955**, *10a*, 541.
- (31) Mataga, N.; Kaifu, Y.; Kazumi, M. *Bull. Chem. Soc. Jpn.* **1955**, *28*, 690.
- (32) Mataga, N.; Kaifu, Y.; Kazumi, M. *Bull. Chem. Soc. Jpn.* **1956**, *29*, 465.
- (33) Baumann, W.; Bischof, H.; Fröhling, J.-C.; Brittinger, C.; Rettig, W.; Rotkiewicz, K. *J. Photochem. Photobiol. A* **1992**, *64*, 49.
- (34) Karelson, M.; Zerner, M. C. *J. Am. Chem. Soc.* **1990**, *112*, 9405.
- (35) Rösch, N.; Zerner, M. C. *J. Phys. Chem.* **1994**, *98*, 5817.
- (36) Lippert, E. In *Organic Molecular Photophysics*; Birks, J. B., Ed.; J. Wiley & Sons: London, 1975; Vol. 2.
- (37) Birks, J. B. In *Photophysics of Aromatic Molecules*; Birks, J. B., Ed.; J. Wiley & Sons Ltd.: London, 1970.
- (38) Cornelissen-Gude, C.; Rettig, W. *J. Phys. Chem.* **1999**, *A102*, 7754.
- (39) Rettig, W. *J. Mol. Struct.* **1982**, *84*, 303.
- (40) Mislow, K. *Acc. Chem. Res.* **1976**, *9*, 26.
- (41) Blount, J. F.; Finocchiaro, P.; Gust, D.; Mislow, K. *J. Am. Chem. Soc.* **1973**, *95*, 7019.
- (42) Hummel, J. P.; Gust, D.; Mislow, K. *J. Am. Chem. Soc.* **1974**, *96*, 3679.
- (43) Brown, N. M. D.; Davidson, F.; Wilson, J. W. *J. Organomet. Chem.* **1981**, *210*, 1.
- (44) Brown, C.; Cragg, R. H.; Miller, T. J.; O'N. Smith, D. *J. Organomet. Chem.* **1981**, *220*, C25.
- (45) Neilson, R. H.; Wells, R. L. *Inorg. Chem.* **1977**, *16*, 7.
- (46) Kovar, R. A.; Waldvogel, G. G. *Inorg. Chem.* **1975**, *14*, 2239.
- (47) Schulz, A.; Kaim, W. *Chem. Ber.* **1989**, *122*, 1863.
- (48) Nöth, H.; Wrackmeyer, B. *Chem. Ber.* **1973**, *106*, 1145.
- (49) Wrackmeyer, B. *J. Organomet. Chem.* **1985**, *297*, 265.
- (50) Bartlett, R. A.; Chen, H.; Dias, R.; Olmstead, M. M.; Power, P. P. *J. Am. Chem. Soc.* **1988**, *110*, 446.
- (51) Olmstead, M. M.; Power, P. P.; Weese, K. J. *J. Am. Chem. Soc.* **1987**, *109*, 2541.
- (52) Bullen, G. J.; Wade, K. *J. Chem. Soc., Chem. Commun.* **1971**, 1122.